Eur. Phys. J. B **32**, 127–136 (2003)
DOI: 10.1140/epjb/e2003-00081-y

THE EUROPEAN PHYSICAL JOURNAL B

Spatial variations of the mean and statistical quantities in the thermal boundary layers of turbulent convection

J. Wang[1,2] and K.-Q. Xia[1,a]

[1] Department of Physics, The Chinese University of Hong Kong, Shatin, Hong Kong, PR China
[2] Institute of Fluid Mechanics, Beijing University of Aeronautics and Astronautics, Beijing, PR China

Received 15 June 2002 / Received in final form 5 February 2003
Published online 14 March 2003 –

Abstract. An experimental study of Rayleigh-Bénard turbulent convection in a cubic cell is presented. We measure the mean temperature profiles, the root mean square (RMS) temperature profiles and the thermal boundary layer thickness for various values of the Rayleigh number Ra and at various positions x along the direction of large-scale circulation (LSC), using water as the working fluid. The scaled mean temperature profiles measured at the same Ra but different x are found to be self-similar, but those measured at different Ra do not show a universal form. In contrast, RMS temperature profiles measured at the same position but different Ra appear to show an invariant form, whereas those with different x but of the same Ra could not be scaled onto a single curve. Irrespective of the measuring positions and Ra, the RMS profiles show a peak value around the boundary layer thickness, and their gradients at bottom surface increase monotonically in the direction of LSC and with increasing Ra.

PACS. 47.27.Te Convection and heat transfer – 44.25.+f Natural convection

1 Introduction

Rayleigh-Bénard convection in the low Rayleigh number regime (*i.e.* near the onset of convection) has served well as an ideal model for the precise study of nonlinear phenomena in dissipative systems. In the high Rayleigh number turbulence regime it has also been shown to be an ideal model for studying turbulence in a closed system. Understanding convection phenomenon in this "simple" system will provide insights into the convection phenomena occurring in the planets, the oceans and the atmosphere. Rayleigh-Bénard convection refers to fluid motion in a closed cell caused by the temperature difference between the cooled top and the heated bottom plates. In comparison to the development of wall boundary layer flow, Rayleigh-Bénard convection also has many flow states: laminar convection, flow stability problem, the transition to turbulence and turbulent convection states. The Rayleigh number Ra may be used to classify the different flow states, $Ra = \alpha g L^3 \Delta T/(\nu\kappa)$, where α is the constant pressure volume expansion coefficient of the fluid, g is the gravitational acceleration, L is the cell height, $\Delta T = T_b - T_t$ is the difference between the bottom and the top plate temperatures, ν is the fluid's kinematic viscosity, and κ its thermal diffusivity.

In the study of turbulent Rayleigh-Bénard convection in the modern era, Malkus is perhaps the first to theoretically investigate this problem in a systematic approach [1], who obtained $Nu \sim Ra^{1/3}$, where Nusselt number Nu is the nondimensional heat flux across the cell. As one of the early pioneers in the experimental studies of Rayleigh-Bénard convection, Townsend [2] measured the mean value and the root mean square of the fluctuating temperature carefully, and found agreement with Markus's theoretical analysis. Later on, Kraichnan [3] obtained the expressions of heat flux, fluctuation velocity and temperature at small and large Prandtl numbers ($Pr = \nu/\kappa$) respectively. From then on, many experiments have been conducted by utilizing different types of convection cells (cylindrical, cubic, and rectangular) and different kinds of fluids (water, air, gaseous helium, mercury, etc.). For a reference of some of these earlier works, please see the review by Siggia [4].

In 1987, Heslot *et al.* [5] carried out a high precision experiment. In their study, the fluid medium was low temperature gaseous helium, and the convection cell was a vertical cylinder with equal diameter and height. By changing the helium density, these authors obtained the experimental Rayleigh number up to 10^{11}, which enabled them to study the Nusselt number dependence of the Rayleigh number over a wide range (in a later experiment, using an aspect ratio $^1/_2$ cell, the Chicago group achieved $Ra \sim 10^{15}$ [6]). According to the temporal temperature signals and $Nu \sim Ra$ curve, the Chicago group divided the Rayleigh-Bénard convection into six regions, *i.e.* the onset of convection ($Ra = 5.8 \times 10^3$), the onset of the oscillatory instability ($Ra = 9 \times 10^4$), the chaotic state ($Ra = 1.5 \times 10^5 \sim 2.5 \times 10^5$), the transition region

[a] e-mail: kxia@phy.cuhk.edu.hk

($Ra = 2.5 \times 10^5 \sim 5 \times 10^5$), the soft turbulence state ($Ra = 5 \times 10^5 \sim 4 \times 10^7$) and the hard turbulence state ($Ra \geq 4 \times 10^7$). The division of soft and hard turbulence is an important contribution to the Rayleigh-Bénard convection problem [7]. In the soft turbulence state, the experimental results indicated that $Nu \sim Ra^{1/3}$, and the probability density for the temperature fluctuation of the center region was Gaussian-like. In contrast to the soft turbulence state, Nu is proportional to $Ra^{0.282}$ in the hard turbulence state, and the probability density for the temperature fluctuation of the center region was exponential. Another feature of the hard turbulence state is that there exists a large-scale circulation that spans the height of the convection cell [8]. For cylindrical cell, the large-scale circulation is confined in an azimuthal plane of the cylinder; and for cubic cell, it is within a vertical diagonal plane [9,10]. To understand the hard turbulence regime in Rayleigh-Bénard convection, many experimental, numerical, and theoretical efforts have been made in the last decade or so. For a recent review on this subject, please see Grossmann and Lohse [11], and Kadanoff [12] for a more pedagogical description on the outstanding issues.

One central focus in the studies of turbulent convection is to determine how the efficiency of heat transport (*i.e.* the Nusselt number Nu) depends on the Rayleigh number Ra, which measures the relative strength of buoyancy over dissipation. More importantly, the main question has been: What is the real mechanism that dictates heat transport, or the Nu and Ra relationship, in the turbulent state of thermal convection? As already mentioned above, a defining feature of hard turbulence has been the power law dependence: $Nu \sim Ra^{\beta}$ with the exponent $\beta = 2/7$. This result is now being challenged both experimentally and theoretically. Questions arise on whether the value of β is $2/7$ [13], or even whether there should be a single power law [12,14]. One thing is clear, however, that these studies have made it more apparent that global measurements, such as Nu *vs.* (Ra, Pr), are far from sufficient for an understanding of the turbulent convection problem. Rather, one needs to make quantitative measurements of the local properties of the temperature and velocity fields, such as boundary layer thickness and shear rate, and test some of the specific predictions and assumptions concerning local quantities made in the various theoretical models. The thermal and viscous boundary layers in the convection cell play key roles in determining the efficiency of heat transport and the various scaling and statistical properties [15]. However, most of the boundary layer measurements were conducted along the central axis of a convection cell [16]. A question naturally arises as to whether the boundary layers are uniform across the horizontal conducting plates on which they reside. The existence of possible spatial nonuniformity of the boundary layers was first suggested by the numerical results of Werne [17] in his two-dimensional (2D) simulation study of the hard turbulence regime. Belmonte *et al.* [18] also pointed out that in order to take into account the heat transported by thermal objects like plumes, the shear produced by the large scale circulation near the boundary should have dependence on horizontal positions and the need to experimentally check the horizontal dependence of both viscous and thermal boundary layer properties. Ching [19] assumed horizontal dependence for both the shear rate and the thermal boundary layer thickness and obtained a scaling relation between the heat flux and the shear rate that agrees better with the direct experimental measurements of these quantities by Xin *et al.* [20] and Xin and Xia [21] than that from the model of Shraiman and Siggia [22]. To investigate the spatial structures of the thermal boundary layer experimentally, Lui and Xia made the first measurement on the positional variation of thermal boundary layer in a cylindrical convection cell and found that the thermal layer indeed has a very strong positional dependence [23]. However it is known that the flow field depends on the geometry of the cell and boundary layers are influenced strongly by the flow field. Recently, Daya and Ecke also presented experimental evidence suggesting that statistics of both the temperature and velocity fields may depend on the geometry of the cell [24]. Moreover, in the work of Lui and Xia, the spatial structure and scaling properties of the RMS temperature fluctuations were not studied and only the mean temperature profiles were investigated [23]. Thus, it is highly desirable that the spatial variations of both the mean and statistical quantities of the thermal boundary layer are investigated and their dependencies on the geometry of the cell be checked. To this end, we have carried our systematic measurements of the mean and RMS temperature profiles, in a cubic convection cell filled with water, with respect to both their positional dependence and Rayleigh number dependence.

The rest of this paper is organized as follows. In Section 2, we give detailed descriptions of our convection cell and the thermistor probe used for local temperature measurements. The experimental results are presented and analyzed in Section 3, which is divided into two parts. Section 3.1 discusses the properties of the profiles of the mean temperature as a function of the vertical distance z from the bottom plate and at various points (to be specified below) along the direction of the large-scale mean flow (which is along one of the diagonals of the bottom plate) and the associate thermal boundary layer thickness; these include the Rayleigh number dependence and the positional variation along the mean flow direction of these quantities. Section 3.2 presents the results on the profiles of the RMS temperature σ as a function of the vertical distance from the bottom plate and at various points along the direction of the large-scale mean flow. The properties of the maximum value (σ_m) of σ at various points along the diagonal and the Ra-dependence of both σ and σ_m will also be presented. We summarize our findings and conclude in Section 4.

2 Experimental

Figure 1 shows a schematic drawing of the convection cell, which is a cube of dimension $L = 25$ cm, thus the aspect ratio is unity. The top and bottom plates were made of

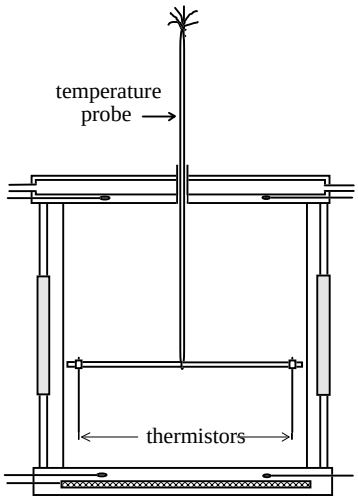

Fig. 1. A schematic drawing of the convection cell used in the experiment. The movable thermistor probe for local temperature measurements is also shown. The four "black dots" inside the top and the bottom plates are imbedded thermistors for measuring temperatures in the respective plates.

copper and their surfaces were gold-plated. The sidewall of the cell consists of four transparent Plexiglas plates. The upper and lower plates are held together by stainless steel posts with Teflon spacers at the eight corners. The temperature of the upper plate is regulated by passing cold water through a cooling chamber fitted on its top. To ensure uniform temperature distribution across the plate, spiral channels are cut on the back of the top plate so that the incoming and the outgoing water are passing each other inside the plate. The lower plate is heated uniformly at a constant rate with an imbedded film heater. The temperature difference ΔT between the two plates is measured by four thermistors imbedded inside the plates, two in each one. The locations of the thermistors at each plate are the same. One is located at the middle of one side of the plate about 45 mm from the edge, the other one is at the symmetric position on the opposite side. They are imbedded at a depth of 4 mm from the fluid-contacting surface of the plates (thickness of the copper plates: 12 mm). The measured relative temperature difference between two thermistors in the same plate is found to be less than 1% for both plates at all Ra, indicating that temperature is uniform across the horizontal plates. In our experiment, water is used as the convecting fluid, and the average temperature of the water in this convection cell is kept near room temperature and only the temperature difference across the cell is changed (the typical values for the average fluid temperature and the temperature difference across the cell are 25 °C and several tens of degrees centigrade, respectively). In this way, the variation of the Prandtl number $Pr = \nu/\kappa$ is kept at minimum ($Pr \approx 7$).

The thermistors used in the local temperature measurements had a diameter of 300 μm and an in-water thermal time constant of 10 ms (AB6E3-B10KA103J, Thermometrics Inc.). In order to access different positions in the convection cell, we used a specially designed temperature probe (see Fig. 1). A rectangular shaped stainless steel rod is soldered perpendicularly on a stainless steel capillary tubing of outer diameter 3.0 mm and inner diameter 2.0 mm. The horizontal rod had a cross-section of 2.2 mm in height and of 0.75 mm in width. A Plexiglas cube of length 4.0 mm can slide freely on the rod. The rod is marked at every 5.0 mm interval to indicate the exact position of the cube. The thermistor is attached at the end of a syringe needle (outer diameter 0.5 mm, length 45 mm) that is fixed to the cube. To move the needle horizontally, two fishing strings of diameter 0.2 mm are tied to the Plexiglas cube. By pulling the strings separately, one can move the needle in either direction along the rod to the desired horizontal position. The leads of the thermistor are fed through the needle, and then, together with the fishing strings, through the tubing to the outside. The tubing is fixed on a vertical translation stage that is mounted right above the filling stem of the convection cell. The stage has a total travel distance of 10.0 cm and a precision of 0.01 mm, and is driven by a computer-controlled stepper motor.

The temperature profile measurement is conducted automatically along the vertical direction, and a 30-minute time series is recorded by a $7^1/_2$-digit multimeter (Keithley Model 2001) at each position. The time-average (or mean) and the RMS values of the local temperature are then obtained from the measured resistance using a calibrated conversion curve. A typical temperature profile consists of more than 30 vertical positions. In the region near the bottom plate surface, there is a large temperature gradient. To obtain valuable and precise information, the measuring step is chosen to be less than 0.1 mm there. After completing one profile measurement, the thermistor is then moved to a different horizontal position and the measurement is repeated. We measured the horizontal variation of the thermal boundary layer along the direction of large-scale circulation (LSC).

To determine the direction of the LSC, we employed the following method. After the convective motion is fully established, a stainless steel tube with a very light string attached to its end is inserted into the convection cell; near the lower plate of the cell, the flow is unidirectional, so the string follows the flow and indicates its direction. It has been found previously [9,20] that once established, the direction of LSC will remain the same for different Rayleigh numbers.

3 Results and discussion

Before presenting the results, let us first define the coordinate system used in the experiment. Let the center of the bottom plate as the origin of right-hand Cartesian coordinates, with the x-axis along one of the diagonals of the bottom plate (the direction of the large-scale flow) and the z-axis points upward. The positive x direction points to the mean flow direction near the bottom plate and the y-axis is defined by the right-hand rule. Note that in the

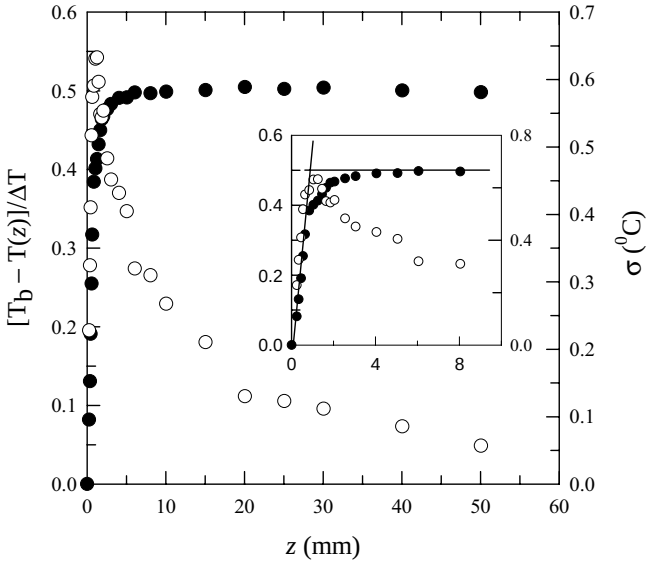

Fig. 2. The scaled mean temperature (dots) and the RMS temperature σ (circles) *vs.* the vertical distance z at $Ra = 3.1 \times 10^9$. The inset shows enlarged portions of the profiles near the boundary layer.

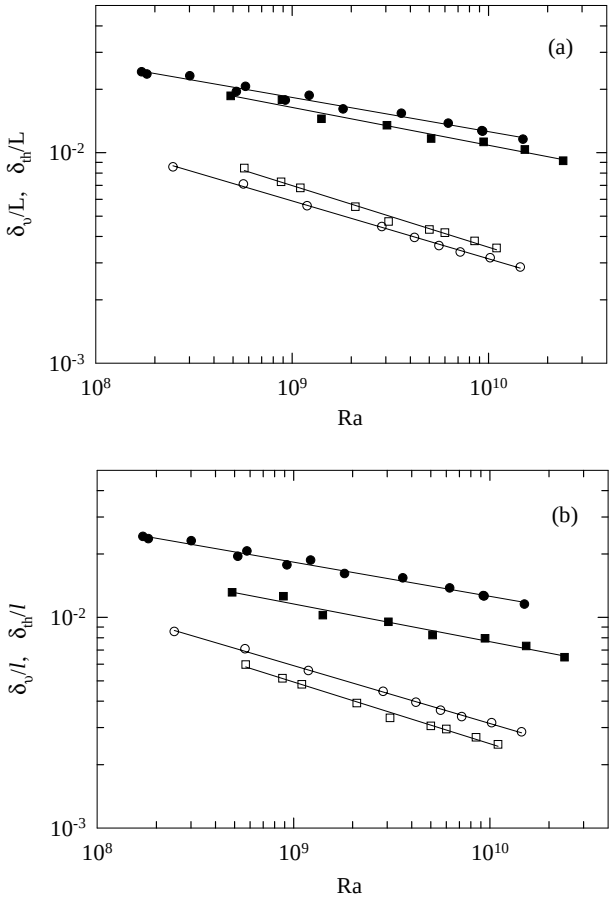

Fig. 3. Viscous boundary layers (solid symbols) and thermal boundary layers (open symbols), measured respectively in a cubic cell (squares) and a cylindrical cell (circles), as *versus* Ra. (a) normalized by the cell height L; (b) normalized by the streamwise dimension l of the bottom plates (see text for the fitting lines).

present experiment no variation with y has been made and all measurements are made with $y = 0$.

Systematical measurements are conducted at fifteen positions on the x-axis. They are $x = 15$, -12, -10, -8, -6, -4, -2 cm (hereafter referred as upstream positions); and $x = 2$, 4, 6, 8, 10, 12, 15 cm (hereafter referred as the downstream positions) on the x-axis, plus the one at the center of the bottom plate ($x = 0$). The varying range of the Rayleigh number in the present experiment is from 5×10^8 to 2.4×10^{10}.

3.1 Mean temperature profiles and thermal boundary layers

Figure 2 shows a typical profile of the time-averaged $T(x = 0, z) = T(z)$ (solid circle) and RMS $\sigma(x = 0, z)$ (open circle) values of the temperature as a function of the distance z along the central axis at $Ra = 3.1 \times 10^9$. In the figure, the mean temperature $T(z)$ has been subtracted from that of the bottom plate T_b and then normalized by the temperature difference ΔT across the convection cell. The insert indicates an enlargement of the region near the plate, where the thermal boundary layer thickness δ_{th} is defined as the distance at which the extrapolation of the linear portion of the profile equals the temperature of the horizontal part. It is seen from the figure that the mean temperature profile can be divided into three regions: a linear portion near the plate where the heat is transported mainly by conduction; a plateau region away from the plate, where temperature gradient is zero and convection dominates; and a transitional region in between. The RMS profile shows a maximum near δ_{th}, which indicates that temperature fluctuations are the strongest in the thermal boundary layer region. This feature will be discussed in detail in Section 3.2.

The Ra-dependence of the thermal boundary layer thickness $\delta_{th}(x = 0) \equiv \delta_{th}(0)$ measured at the center ($x = 0$, $y = 0$) of the bottom plate for the present cubic cell can be fitted to a power-law which gives $\delta_{th}(0) = 575 Ra^{-0.28}$ (mm). To see whether the scaling or amplitude of the boundary layers depend on the cell geometry, we compare this result with that obtained from a cylindrical cell also of aspect ratio one (with height equal to 19.6 cm). Figure 3 plots the normalized thermal layer thickness $\delta_{th}(0)/L$ for the cubic cell obtained in the present work (open squares) and that for the cylindrical cell (open circles) from reference [23], which corresponds to $\delta_{th}(0) = 425 Ra^{-0.285}$ (mm). Also plotted in the figure are the viscous boundary layer thickness $\delta_v(0)/L$ obtained at the center of the bottom plate for the cubic cell (solid squares, fitting corresponds to $\delta_v(0)/L = 0.69 Ra^{-0.18}$) and the cylindrical cell (solid circles, fitting corresponds to $\delta_v(0)/L = 0.51 Ra^{0.16}$) respectively. The cubic cell result was measured by Qiu and Xia [10], in which the same cell was used as the current experiment. The cylindrical

cell result was measured by Xin *et al.* [20] using the same cell as that in reference [23]. It is seen clearly from the figure that the scaling behavior is the same for the cubic and cylindrical cells and it is true for both the viscous and the thermal layers. On the other hand, the amplitudes appear to depend on cell geometry for both the viscous and the thermal layers. Grossmann and Lohse suggested recently that the relevant streamwise length scale for the plates should be the width of the plate l [25]. In Figure 3b we plot the same boundary layers shown in 3a but normalized by l instead of by L, with the same symbols. Here $l = \sqrt{2}L$ for the cubic cell since the flow here is along the diagonal near the plates and $l = L$ for the cylindrical cell. Note that $L = 25$ and 19.6 cm for the cubic and cylindrical cells, respectively. We see that with this normalization, the amplitudes for the boundary layers still depend on cell geometry. But now both the thermal and viscous layer thicknesses for the cubic cell are thinner than those for the cylindrical cell. We stress that it is not our intention to test which normalization is the more appropriate one to use and nor can we tell. We make these comparisons to show that the amplitudes for both the thermal and viscous boundary layers depend on the cell geometry irrespective of what normalization is used, while the scalings with Ra are the same. Note that this is not necessarily contradicting the findings by Daya and Ecke that the scalings of fluctuating quantities depend on cell shape [24]. Note also that Qiu and Xia [26] have reported previously that the measured Nusselt number Nu for the cubic and the cylindrical cells are the same in terms of both amplitude and scaling with Ra. Since Nu can be related to the global average of the position-dependent boundary layer thickness (see, for example, Eq. (3) in Ref. [23]), the fact that the two cells have the same Nu but different thermal layer thickness simply implies that the spatial structures of the boundary layer are different for the two cells. This, of course, should come as no surprise and will be seen below explicitly.

Now we focus our attention on the positional dependence of the thermal boundary layer. Figure 4 shows the measured thermal layer thickness $\delta_{th}(x)$ as a function of the coordinate x along the direction of the LSC, for four different values of Ra. In the figure, $\delta_{th}(x)$ has been normalized by the thickness $\delta_{th}(0)$ measured at the center of the bottom plate, and x by one half of the cell diagonal $\sqrt{2}L/2 = 0.707L$. It is seen from Figures 4a and b (for $Ra = 1.1\times10^9$ and 3.1×10^9 respectively) that there exists a minimum value of the boundary layer thickness $\delta_{th}(x)$ in the central region of the bottom plate, but the distribution is asymmetric and with increasing Ra the position of its minimum is shifted from upstream ($x < 0$) to downstream ($x > 0$) of the LSC. These features of the thickness profile are quite different from those seem in a cylindrical cell, where a symmetric "V" shape of the boundary layer profile is found [23]. We attribute this difference to the effect of the sharp corners in the cubic cell on the flow, which influences the temperature field. An asymmetric distribution of $\delta_{th}(x)$ has also been found in a numerical study [17], where a square geometry was used. Thus

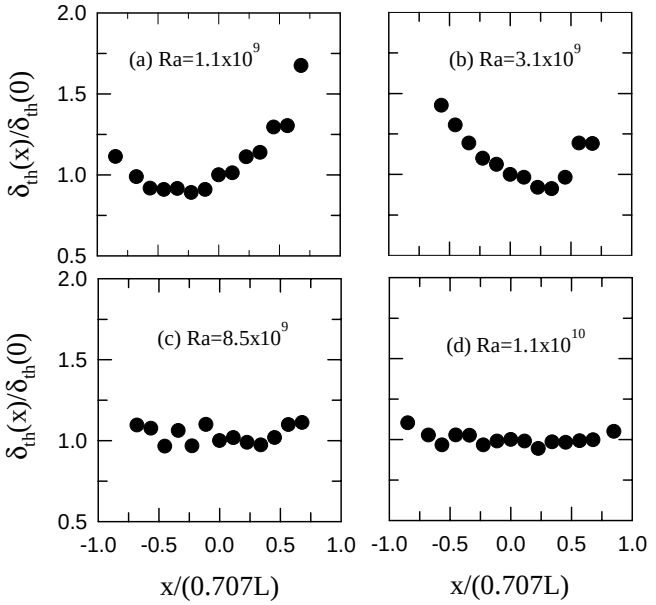

Fig. 4. Normalized thermal boundary layer thickness *vs.* normalized positions x along the direction of LSC for four values of Ra.

we see an example of cell geometry influences the characteristics of thermal boundary layer structures in turbulent convection. For $Ra \geq 8.5\times10^9$, it is seen from Figures 4c and 4d that, except very close to the sidewall region, the thermal boundary layer thickness remains nearly constant. Lui and Xia [23] pointed out that, with increasing Ra, the thermal boundary layer distribution would eventually become uniform in the center of the bottom plate. Although the trends of thermal boundary layer thickness distributions are the same for the two experiments, the transitional Ra is seen to be different in these cases. This is another manifestation of how cell geometry influences the spatial structures and temperature field.

We examine below how the measured temperature profiles vary with position. Figure 5 shows the scaled temperature profiles measured at various positions along the direction of LSC. In Figure 5a only portions near the boundary layer region with $z/\delta_{th} \leq 5.0$ are shown and they are all measured at the same Ra ($=6.0\times10^9$). For other values of Ra, we obtain the same result. It is seen from this figure that, for positions both upstream and downstream of $x = 0$, the measured temperature profiles all collapse onto a single curve (see Fig. 5b for symbol legends). This feature has also been observed in the experiment using a cylindrical cell [23]. Thus, it appears that the mean temperature profiles can be scaled to collapse onto a single curve (in the range of $z/\delta_{th} \leq 5.0$) irrespective of the cell geometry. In the 2-D numerical simulation of hard turbulence, Werne [17] found that the temperature profile is self-similar only in the range of $z/\delta_{th} \leq 1.0$. Besides this small region, his results indicate that the temperature profiles change with both measured position and Ra. To examine the positional dependence of temperature profiles over a wider range, we show in Figure 5b the

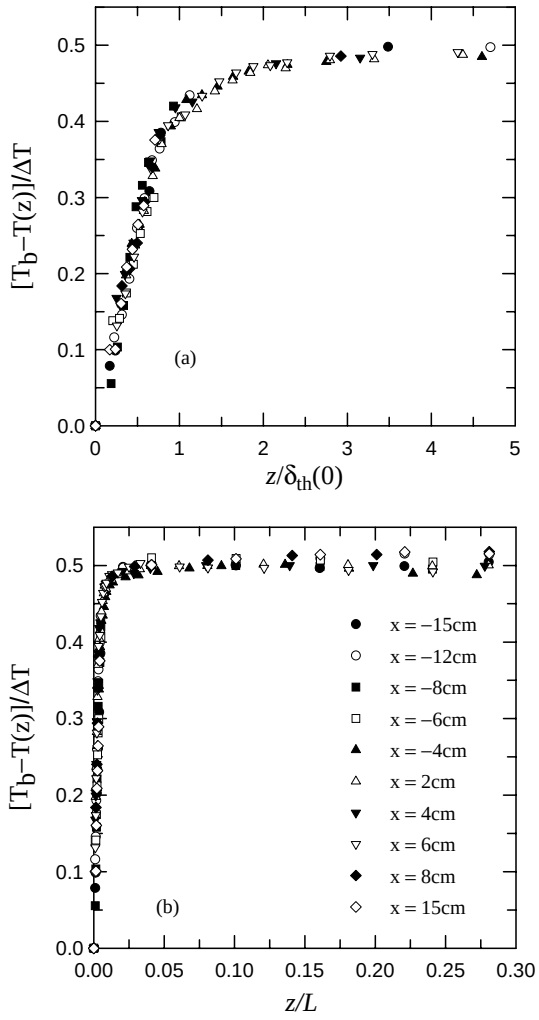

Fig. 5. (a) Near-boundary portion of the scaled temperature profiles measured at various positions x along the direction of LSC at $Ra = 6.0 \times 10^9$. (b) The complete profiles of those in (a), the symbol legends also apply to (a).

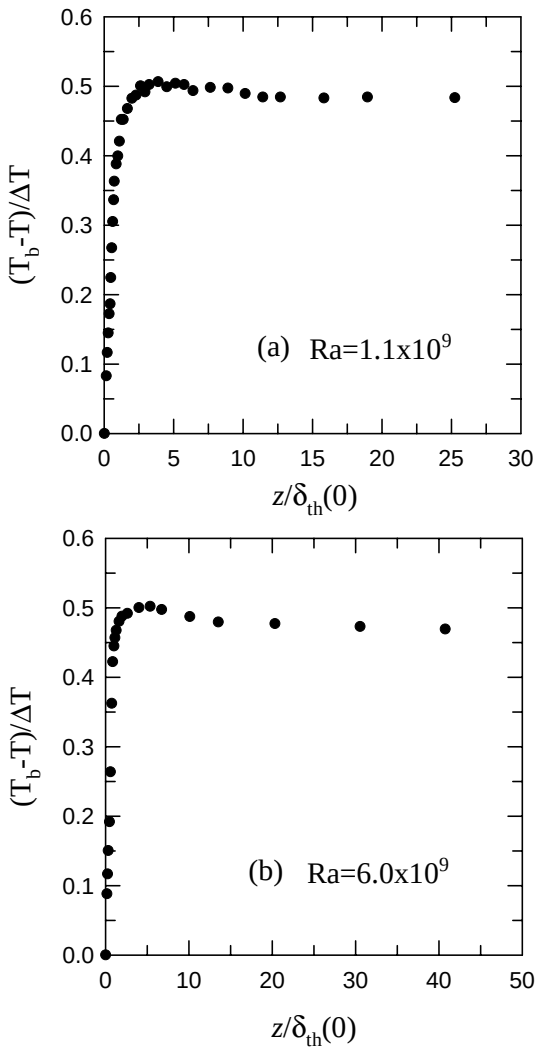

Fig. 6. Scaled temperature profiles showing the existence a temperature inversion and for which δ_{th} is the smallest: (a) $x = -2$ cm, $Ra = 1.1\times10^9$; (b) $x = -10$ cm, $Ra = 6.0\times10^9$.

complete profiles of those shown in (a) (note that the horizontal axis is now the vertical distance z scale by the cell height L and z/L corresponds roughly to $z/\delta_{th} = 75$). It is seen from this figure that in the bulk region some of the scaled temperature profiles start to depart from the mean value $[T_b - T(z)]/\Delta T = 0.5$, which shows that the temperature profiles are self-similar only in regions not far from the boundary layers. Moreover, we also found that there exists an apparent temperature inversion just outside the bottom boundary layer region (*i.e.* the mean temperature near the hot boundary layer is *colder* than that in the bulk region) in the temperature profiles measured at positions of thinnest boundary layers, *i.e.* at values of x for which $\delta_{th}(x)$ is minimum. Figure 6 shows two such examples. This inversion was not seen in cylindrical cells [23] and thus is a consequence of the particular geometry of the cell. Apparently this inversion is caused by an "excessive" amount of cold plumes brought from the top plate by the particular flow pattern that is dictated by the cell geometry. Please note that in Figure 6 only a portion of the profile close to the boundary layer is shown (for example, in Fig. 6b, the largest value of z/δ_{th} is about 40, which is about 4 cm since the corresponding boundary layer thickness is about 1 mm), thus it appears that $(T_b - T)/T$ is below 0.5. But in the complete profiles the value of 0.5 for $(T_b - T)/T$ will be recovered near the central part of the cell.

We now look at scaling properties of the temperature profiles with respect to the Rayleigh number. Figure 7 plots several profiles measured at the center of the bottom plate with their values of Ra indicated on the graph. It is seen that the shape of the profiles in the 'transitional' region varies with Ra in a monotonic fashion. This is in agreement with the results obtained in cylindrical cell [23], but in contrast to the results from velocity measurements where it was found that velocity profiles measured at different values of Ra have an invariant form [10,20]. This implies that the effects of Ra on mean temperature and velocity distributions are different. It should be noted

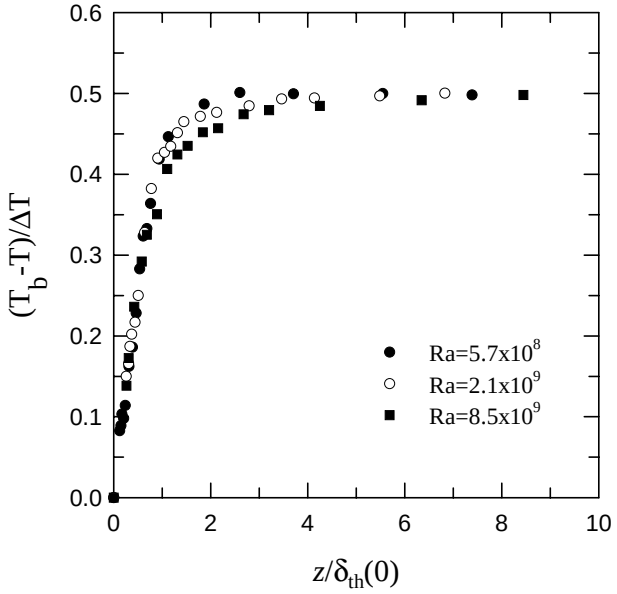

Fig. 7. Scaled temperature profiles measured at the central axis ($x = y = 0$) of the cell, at various Ra.

that, in contrast to our results, Belmonte, Tilgner and Libchaber [27] found (also in a cubic convection cell) that temperature profiles of different Ra could be scaled to collapse onto a single curve (but Ra in that experiment varied only over a narrow range, all around 10^8). Lui and Xia [23] attributed this difference to the large difference in Prandtl number in the two experiments. In the experiment reported in reference [27], pressurized gas was used as the working fluid and the Prandtl number was about 0.7. To settle this difference, it seems future experiments need to be conducted in low Pr fluids and over a wide range of Ra.

3.2 Properties of the RMS temperature profiles

We now present results for the RMS temperature profile $\sigma(x, z)$. First, we look at the profiles $\sigma(z)$ measured at the central axis ($x = 0$) for different values of Ra. Figure 8a shows a plot of nine profiles with the vertical distance from bottom plate z scaled by the boundary layer thickness $\delta_{th}(0, 0)$ at the center of the bottom plate ($x = y = 0$). We see from the figure that the maximum value, σ_m, of the RMS profile increases with Ra, this means that the temperature field become more turbulent with increasing Ra. The more prominent feature is that σ_m occurs at about $z/\delta_{th}(0, 0) = 0.8$ regardless the value of Ra (in fact the scatter of the data does not allow us to distinguish whether it is 0.8 or 1.0, but for comparison with Figure 10 below, we use 0.8 for the sake of discussion). It is seen from Figure 2 that σ_m occurs approximately at the upper edge of the thermal boundary layer, now we see that this is true for all the measured profiles across a wide range of Ra. In fact, we may now define the peak position of σ as where the thermal boundary layer is located. Recall that the definition we took for δ_{th} is an operational one and since σ_m occurs at $0.8\delta_{th}$

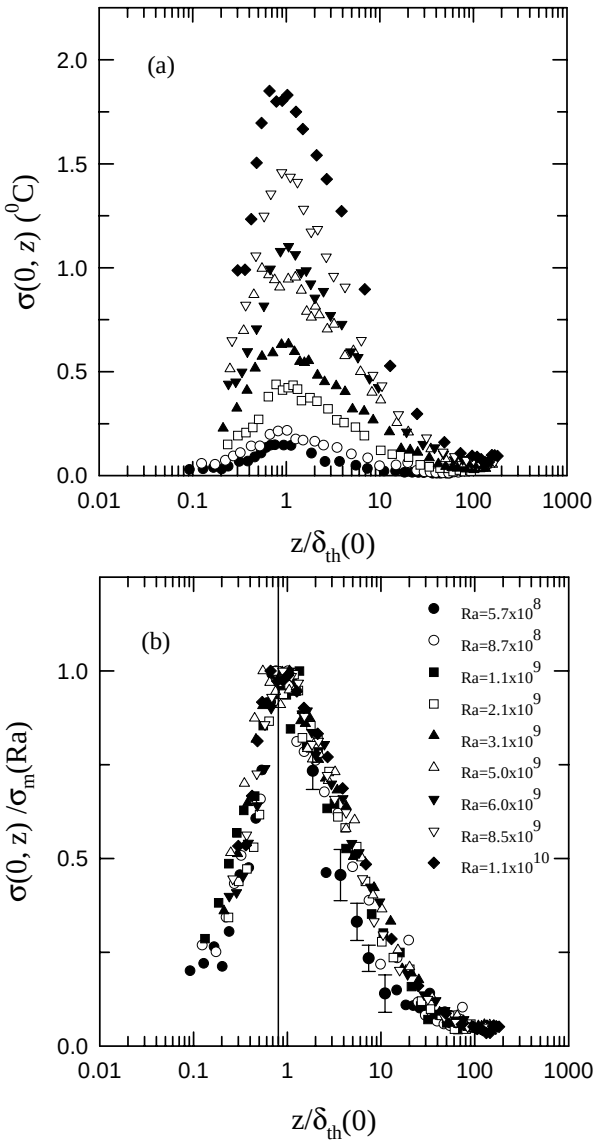

Fig. 8. (a) Profiles of the RMS temperature fluctuations measured at the central axis ($x = y = 0$) of the cell, and at various Ra from 5.7×10^8 to 1.1×10^{10}. (b) The same profiles scaled by σ_m for their respective values of Ra, the symbol legends also apply to (a). The dashed line indicates the approximate position of the maximum value σ_m.

for all Ra, the two definitions will give, apart from a constant shift, essentially the same results. It should also be noted that the position $z/\delta_{th}(0, 0) = 0.8$ is a characteristic point where the coherent structure should be detected as those done for wall turbulence [28,29]. Figure 8b plots the scaled RMS profiles σ/σ_m with the scaled vertical distance $z/\delta_{th}(0)$ from the lower plate, here we see that over a wide range of Ra and within the data scatter these profiles appear collapse onto a single curve irrespective of Ra. This is in contrast to the profiles of the mean temperature where systematic variations of shape with Ra are clearly observed (Fig. 7). Because the RMS data are much more noisy than the mean profile, the feature will need to be verified with more accurate measurements, which presumably

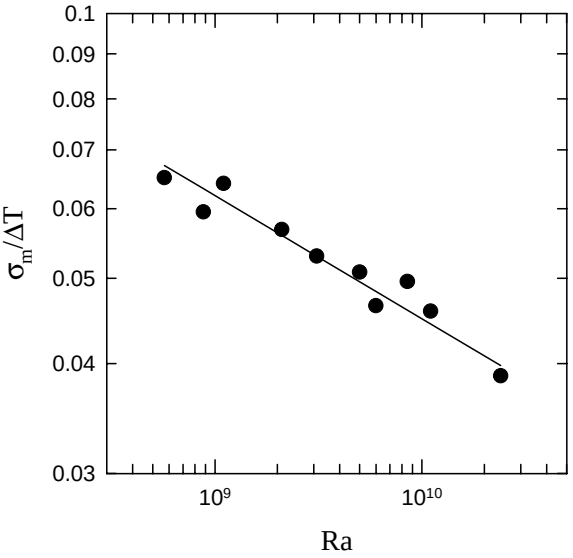

Fig. 9. Scaled maximum value σ_m of RMS temperature profile measured at the central axis of the cell *vs.* Ra. The solid line is a power law fit: $\sigma_m/\Delta T = 1.13Ra^{-0.14}$.

will entail much longer time averages in data acquisitions. If proven to be true, it will mean that the 'fluctuating quantities' are more universal than mean quantities in turbulent convection. We next look at the Ra-dependence of σ_m for profiles measured at cell center ($x = 0$). Figure 9 shows σ_m normalized by the temperature difference ΔT against Ra in log-log plot where the solid line represents a best fit to the data: $\sigma_m/\Delta T = 1.13Ra^{-0.14\pm0.03}$. To our knowledge, the Ra-dependence of σ_m has not been obtained before. It is also interesting that σ_m has the same exponent as the RMS temperature fluctuation σ_c measured at the cell center [7,30] of a cylindrical cell. Because the data in Figure 9 is somewhat scattered, more accurate measurements are certainly needed to verify the above exponent.

We now examine the spatial variations of the profiles of the RMS temperature σ. Figure 10 shows a group of profiles of σ measured at various positions along direction of the LSC at $Ra = 6.0 \times 10^9$, with (a) those from upstream positions and (b) downstream positions (note that the mean flow is along the x-axis and in the positive direction). Similar to Figure 8b, here $\sigma(x, z)$ is normalized by its maximum value $\sigma_m(x)$ and the distance z by the thermal layer thickness $/\delta_{th}(x)$, all corresponding to the same position x. Both (a) and (b) show that within the uncertainty of the experiment σ_m occurs at $z/\delta_{th}(x, 0) \approx 0.8$ for different values of x, as indicated by the dashed line in the figure. When combining this with the result shown in Figure 8, we see that the measured σ_m occurs at $z \approx 0.8\delta_{th}(x, 0)$ irrespective of the values of Ra and the position x, which further support our earlier conclusion that these two quantities represent essentially the same length scale. It is also clear from the figure that these profiles could not be scaled to collapse on a single curve (*i.e.* when the vertical axis is normalized by σ_m for the respective x positions), even for small ranges of z/δ_{th}.

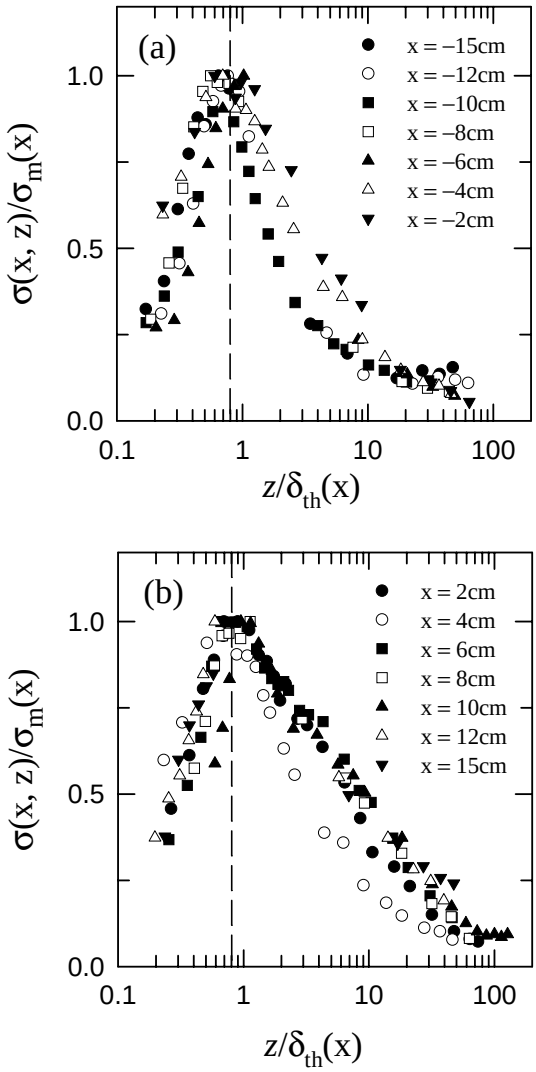

Fig. 10. Profiles of the RMS temperature fluctuations measured at various positions x along the direction of LSC and $Ra = 6.0 \times 10^9$: (a) upstream region ($x < 0$) and (b) downstream region ($x > 0$). As in Figure 8, the dashed lines indicate the approximate position of the maximum value σ_m.

Whereas in Figure 8, it is seen that profiles for different values of Ra but at the same x position collapse reasonably well within the uncertainty of the experiment. Thus, the RMS profiles appear to show opposite behavior in contrast to the mean temperature profiles, where invariance with respect to position (Fig. 5) but not with respect to Ra (Fig. 7) has been observed. Given the fact that the RMS data are more scattered than the mean values, we believe that further and more precise measurements are needed to unambiguously establish these results.

In Figure 11 we show how σ_m varies with position and with Ra, where it is seen that σ_m increases with Ra. Moreover, for each Ra the distribution of σ_m appears to have an asymmetrical "V" shape about the central axis, with upstream slope greater than the downstream value for the higher Ra profiles. Note that the minimum position in the profile of the lowest $Ra(1.1 \times 10^9)$ appears to have shifted

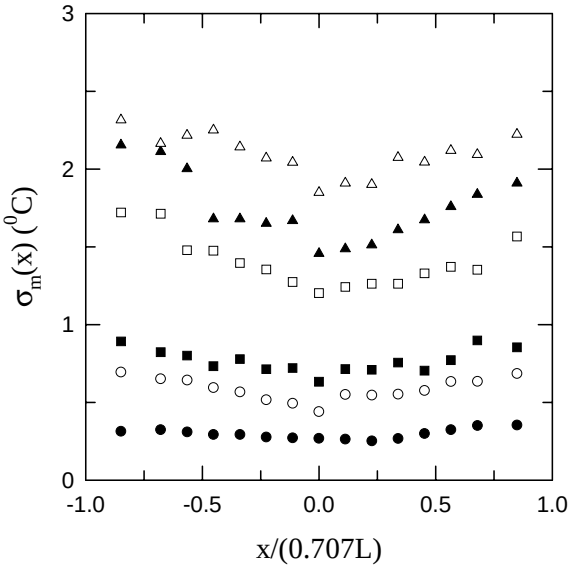

Fig. 11. The profiles of σ_m along the direction of LSC for various Ra, the x-axis is scaled by half of the diagonal length of the bottom plate: ● $Ra = 1.1 \times 10^9$; o $Ra = 2.1 \times 10^9$; ■ $Ra = 3.1 \times 10^9$; □ $Ra = 6.0 \times 10^9$; ▲ $Ra = 8.5 \times 10^9$; and △ $Ra = 1.1 \times 10^{10}$.

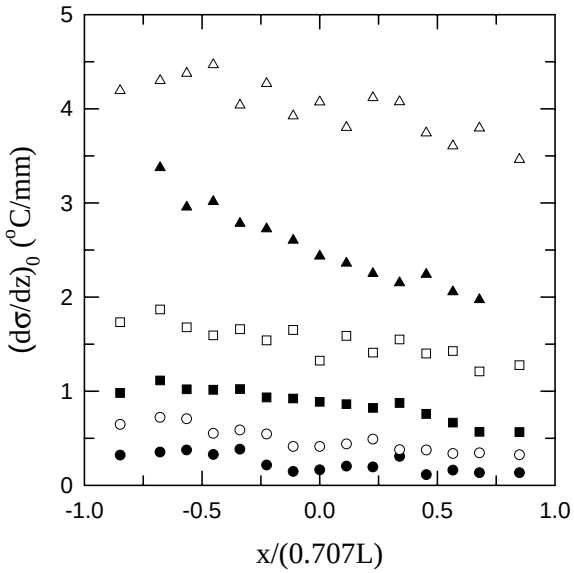

Fig. 12. Profiles of the vertical gradient of the RMS temperature at bottom plate ($\partial\sigma\partial z|_{z=0}$), as functions of the normalized distance along the direction of LSC for various values of Ra. The symbols are the same as those in Figure 11.

from $x = 0$ to a larger value (the figure is somewhat compressed, but an expanded view reveals this more clearly), it remains to be seen if this is a trend for lower values of Ra.

Figure 12 shows how the gradient of σ at bottom plate ($\partial\sigma/\partial z|_{z=0}$) varies along the direction of the LSC for different values of Ra. It is seen that there is a trend of $\partial\sigma\partial z|_{z=0}$ decrease almost monotonically along the mean flow direction from upstream to downstream (the vertical axis is somewhat compressed, but an expanded view will reveal this trend more clearly). It is seen that the gradient increases with increasing Ra in both its magnitude and its slope with respect to x (the exception may be that for $Ra = 1.1 \times 10^{10}$, where the slope appears to be smaller than those with lower Ra). We think the larger gradient at upstream positions may be due to the large number of cold plumes brought down by the mean flow (LSC) from the top plate. As these hot plumes traveled downstream along the bottom plate, they get mixed with some of the hot plumes there, resulting in a reduction in the gradient of σ.

4 Summary

Temperature time-series at various values of Ra and at various positions along the direction of large-scale circulation (LSC) of a cubic convection cell have been measured, with the control parameter Ra spanning the range of $5.7 \times 10^8 \sim 1.1 \times 10^{10}$. We obtain the (time-averaged) mean temperature profiles and the profiles of the root-mean-square (RMS) standard deviation of the fluctuating temperature. From these, the thermal boundary layer thickness and its spatial and Ra variations are obtained. Specifically, the following are observed.

(i) When the mean temperature profiles are properly normalized, two distinct features emerge that further support the earlier results found in a cylindrical convection cell. For the same Ra, the scaled mean temperature profiles measured at different horizontal positions along the mean flow are found to be self-similar in the range of $z/\delta_{th} \leq 10.0$. For the same position but different Ra, the scaled profiles are found to be Ra-dependent, *i.e.* they cannot be brought to collapse onto a single curve.

(ii) The thermal boundary layer thickness varied significantly in the direction of large-scale circulation, and there exists a "valley" for $Ra \leq 6.0 \times 10^9$. In contrast to the findings in the cylindrical cell, the "thickness profiles" are asymmetric. Moreover, position of the minimum of the profile (or valley) appears to shift with Ra. For $Ra \leq 2.1 \times 10^9$, the position of valley is in the upstream side; and for $Ra \geq 3.1 \times 10^9$, it is in the downstream side. When $Ra \geq 8.5 \times 10^9$, the thickness tends to become uniform. All these features are different than those observed in a cylindrical cell, showing evidence of the geometry of the cell influences the structures of the temperature field.

(iii) For positions corresponding to the valley of the thermal boundary layer thickness profiles, the normalized mean temperature distribution has an inversion in the region near bottom plate. We think this inversion is caused by an "excessive" amount of cold plumes brought from the top plate by the particular flow pattern that is influenced by the cell geometry.

(iv) In contrast to the mean temperature case, the RMS temperature profiles measured at various Ra but at the same location appear to show an invariant form, *i.e.* they can be brought to collapse onto a single curve

when properly scaled. Whereas profiles of the same value of Ra but measured at different positions, along the bottom plate in the mean flow direction, could not be scaled to collapse onto a universal curve.

(v) The peak value (σ_m) of RMS temperature profiles is found to be located at $z/\delta_{th} = 0.8$ irrespective of the Rayleigh number Ra and the measuring position x. The profiles of σ_m is found to also have an asymmetric "V" shape about the central axis, Moreover, σ_m measured at various Ra appear to follow a power law $\sigma_m/\Delta T \sim Ra^{-0.14}$.

(vi) The gradient of σ at the bottom plate ($\partial\sigma\partial z|_{z=0}$) is found to be decreasing monotonically along the direction of the LSC, from upstream to downstream. We attribute this to the interactions between plumes and the mean flow.

The experimental results presented in this paper demonstrate that the hard-turbulence regime in thermal convection is a complex phenomena with many rich features, and most of the existing models provide only a partial understanding of this turbulence state. The data presented here provide important information and constraints for the formulation of future theoretical models. Clearly, to have a complete understanding of the interplay between the large-scale circulation and the heat flux, one needs to map out the full spatial structure of the temperature and the velocity fields in the boundary layer region in future experiments.

We thank S.L. Lui, X.L. Qiu and S.Q. Zhou for their help in the experiments. We gratefully acknowledge support of this work by the Research Grants Council of Hong Kong SAR under Grant No. CUHK4242/01P.

References

1. W.V.R. Malkus, Proc. R. Soc. London A **225**, 196 (1954)
2. A.A. Townsend, J. Fluid Mech. **5**, 209 (1959)
3. R.H. Kraichnan, Phys. Fluids **5**, 1374 (1962)
4. E.D. Siggia, Ann. Rev. Fluid Mech. **26**, 137 (1994)
5. F. Heslot, B. Castaing, A. Libchaber, Phys. Rev. A **36**, 5870 (1987)
6. X. Wu, A. Libchaber, Phys. Rev. A **45**, 842 (1992)
7. B. Castaing, G. Gunaratne, F. Heslot, L. Kadanoff, A. Libchaber, S. Thomae, X. Wu, S. Zaleski, G. Zanetti, J. Fluid Mech. **204**, 1 (1989)
8. R. Krishnamurti, L.N. Howard, Proc. Natl. Acad. Sci. **78**, 1981 (1991)
9. G. Zocchi, E. Moses, A. Libchaber, Physica A **166**, 387 (1990)
10. X.L. Qiu, K.Q. Xia, Phys. Rev. E **58**, 5816 (1998)
11. S. Grossmann, D. Lohse, J. Fluid Mech. **407**, 27 (2000)
12. L.P. Kadanoff, Physics Today **54**, 34 (2001)
13. J.J. Niemela, L. Skrbek, K.R. Sreenivasan, R.J. Donnelly, Nature **404**, 837 (2000)
14. X. Xu, K.M.S. Bajaj, G. Ahlers, Phys. Rev. Lett. **84**, 4357 (2000)
15. For a review on the roles played by the thermal and viscous boundary layers and their relationship, please see, for example, reference [11] and the extension of the theory to the case of very high Prandtl numbers by the same authors [Phys. Rev. Lett. **86**, 3316 (2001)]
16. A. Tilgner, A. Belmonte, A. Libchaber, Phys. Rev. E **47**, R2253 (1993)
17. J. Werne, Phys. Rev. E **48**, 1020 (1993)
18. A. Belmonte, A. Tilgner, A. Libchaber, Phys. Rev. E **50**, 269 (1994)
19. E.S.C. Ching, Phys. Rev. E **55**, 1189 (1997)
20. Y.-B. Xin, K.-Q. Xia, P. Tong, Phys. Rev. Lett. **77**, 1266 (1996)
21. Y.-B. Xin, K.-Q. Xia, Phys. Rev. E **56**, 3010 (1997)
22. B.I. Shraiman, E.D. Siggia, Phys. Rev. A **40**, 3650 (1990)
23. S.-L. Lui, K.-Q. Xia, Phys. Rev. E **57**, 5494 (1998)
24. Z.A. Daya, R.E. Ecke, Phys. Rev. Lett. **87**, 184501 (2001)
25. S. Grossmann, D. Lohse, submitted to J. Fluid Mech. (2003)
26. X.-L. Qiu, K.-Q. Xia, Phys. Rev. E **58**, 486 (1998)
27. A. Belmonte, A. Tilgner, A. Libchaber, Phys. Rev. Lett. **70**, 4067 (1993)
28. A.V. Johansson, P.H. Alfredsson, J. Fluid Mech. **122**, 295 (1982)
29. W.W. Willmarth, S.S. Lu, J. Fluid Mech. **55**, 65 (1972)
30. K.-Q. Xia, S.-L. Lui, Phys. Rev. Lett. **79**, 5006 (1997)